Title

pH-Weighted amine chemical exchange saturation transfer echo planar imaging visualizes infiltrating glioblastoma cells

Journal

Neuro-Oncology, 26(1)

ISSN

1522-8517

Authors

Patel, Kunal S
Yao, Jingwen
Cho, Nicholas S
et al.

Publication Date

2024-01-05

DOI

10.1093/neuonc/noad150

Peer reviewed

Neuro-Oncology
26(1), 115–126, 2024 | https://doi.org/10.1093/neuonc/noad150 | Advance Access date 18 August 2023

pH-Weighted amine chemical exchange saturation transfer echo planar imaging visualizes infiltrating glioblastoma cells

Kunal S. Patel, Jingwen Yao, Nicholas S. Cho, Francesco Sanvito, Kaleab Tessema, Alvaro Alvarado, Lindsey Dudley, Fausto Rodriguez, Richard Everson, Timothy F. Cloughesy, Noriko Salamon, Linda M. Liau, Harley I. Kornblum, and Benjamin M. Ellingson

All author affiliations are listed at the end of the article

Corresponding Author: Benjamin M Ellingson, PhD, Director, UCLA Brain Tumor Imaging Laboratory, Professor, Radiology, Psychiatry, and Neurosurgery, David Geffen School of Medicine, University of California, Los Angeles, 924 Westwood Blvd., Suite 615, Los Angeles, CA 90024, USA (bellingson@mednet.ucla.edu).

Abstract

Background. Given the invasive nature of glioblastoma, tumor cells exist beyond the contrast-enhancing (CE) region targeted during treatment. However, areas of non-enhancing (NE) tumors are difficult to visualize and delineate from edematous tissue. Amine chemical exchange saturation transfer echo planar imaging (CEST-EPI) is a pH-sensitive molecular magnetic resonance imaging technique that was evaluated in its ability to identify infiltrating NE tumors and prognosticate survival.

Methods. In this prospective study, CEST-EPI was obtained in 30 patients and areas with elevated CEST contrast ("CEST+" based on the asymmetry in magnetization transfer ratio: MTRasym at 3 ppm) within NE regions were quantitated. Median MTRasym at 3 ppm and volume of CEST + NE regions were correlated with progression-free survival (PFS). In 20 samples from 14 patients, image-guided biopsies of these areas were obtained to correlate MTRasym at 3 ppm to tumor and non-tumor cell burden using immunohistochemistry.

Results. In 15 newly diagnosed and 15 recurrent glioblastoma, higher median MTRasym at 3ppm within CEST + NE regions ($P = .007$; $P = .0326$) and higher volumes of CEST + NE tumor ($P = .020$; $P < .001$) were associated with decreased PFS. CE recurrence occurred in areas of preoperative CEST + NE regions in 95.4% of patients. MTRasym at 3 ppm was correlated with presence of tumor, cell density, %Ki-67 positivity, and %CD31 positivity ($P = .001$; $P < .001$; $P < .001$; $P = .001$).

Conclusions. pH-weighted amine CEST-EPI allows for visualization of NE tumor, likely through surrounding acidification of the tumor microenvironment. The magnitude and volume of CEST + NE tumor correlates with tumor cell density, degree of proliferating or "active" tumor, and PFS.

Key Points

(1) Amine CEST-EPI shows differential MTRasym in non-enhancing areas in glioblastoma relative to normal-appearing white matter.

(2) Amine CEST-EPI MTRasym ≥ 1.5 % correlates with pathological diagnosis of infiltrating tumor.

Standard of care for treatment of IDH wild-type World Health Organization (WHO) IV glioblastoma[1] includes maximal safe resection followed by concomitant temozolomide and radiation therapy to the surgical bed[2] followed by adjuvant temozolomide. Both surgical resection[3–5] and radiotherapy[6] focus on removal or treatment of the contrast-enhancing (CE) portion of the tumor, which is known to contain the most aggressive portion of the tumor[7–9] and is a strong prognostic factor for patient survival.[7,10] However, given the invasive nature of diffuse gliomas[11] and the most common area

Importance of the Study

Visualizing infiltrating tumor cells beyond the contrast-enhancing portion of glioblastoma has been technically difficult. Amine chemical exchange saturation transfer is a pH-sensitive magnetic resonance imaging technique that demonstrates contrast in the non-enhancing area surrounding the enhancing bulk of tumor. In this study, we prospectively show this novel technique correlates with presence and density of infiltrating glioblastoma cells as well as progression-free survival. The ability to visualize these cells may allow for improved local extent of resection, targeted radiotherapy, and earlier identification of recurrence.

of recurrence occurring at the margins of the resection cavity,[12] residual infiltrating glioma cells clearly exist beyond the CE[9] and are likely responsible for treatment resistance and the poor prognosis in glioblastoma.

Surgeons have long examined possibility of resecting the infiltrating, non-enhancing (NE) component of glioblastoma in order to improve patient outcomes.[10] Because infiltrating glioma cells cannot be reliably distinguished on gross inspection, resection of tumor is largely guided by intraoperative neuronavigation linked to preoperative magnetic resonance imaging (MRI). Therefore, surgical resection of infiltrating NE glioma, described in the literature as "supratotal or supramarginal resection,"[13,14] is dependent solely on hyperintensity on T2-weighted or T2-weighted fluid-attenuated inversion recovery (FLAIR) sequences, which contains an unknown mixture of both NE tumor and vasogenic edema. This makes quantitation of supratotal resection difficult and imprecise, as the AANS/CNS consensus definition is gross total resection of CE area plus "some non-contrast enhancement."[13] Given the urgent need to target infiltrating glioma for surgical and treatment planning, an MRI technique that can more precisely identify and visualize NE tumor within T2/FLAIR hyperintense areas of glioblastoma would be of great clinical value.

Multiple imaging modalities have been studied in regards to identifying NE tumor, including: Fluorodeoxyglucose (FDG) positron emission tomography,[15–17] diffusion-weighted imaging,[18,19] diffusor tensor imaging,[20] perfusion weighted imaging,[21] and magnetic resonance spectroscopy.[22,23] These studies have been limited to correlation studies and have been used to differentiate glioma from alternative diagnoses, and estimate prognosis. However, lack of resolution and pathologic confirmation limits the validity of these techniques. Amine chemical exchange saturation transfer echo planar imaging (CEST-EPI) is a noninvasive MRI sequence that provides contrast based on the exchange rate of amine protons on amino acids, including neurotransmitters, with protons in bulk water.[24–26] The exchange rate of these fast-exchanging amine protons are base-catalyzed and phosphate-dependent,[27] making amine CEST-EPI contrast highly dependent on extracellular acidity, particularly within areas of high amino acid concentration and elevated T2, both known to occur within NE tumor. Consistent with physics simulations, we have shown the asymmetry in the magnetization transfer ratio at 3 parts per million from water resonance, or the resonance frequency for amine protons (MTR_{asym} *at 3 ppm*), is sensitive to extracellular acidity, is dependent on underlying molecular characteristics of specific brain tumor subtypes, and can be used to quantify response to various treatments.[26,28,29] We theorize that pH-weighted amine CEST-EPI may be useful for visualizing areas of infiltrating NE glioblastoma by focusing on the unique way infiltrating tumor cells increase the acidity of the surrounding microenvironment through elevated glycolysis leading to increased lactic acid production.[30–32]

In the current study, we examine amine CEST-EPI in a surgical cohort of glioblastoma patients, identify areas of elevated tumor acidity within NE tumor, correlate these measurements with pathology and progression-free survival, then prospectively acquire image-guided targeted biopsies to quantitate cell type and characteristics of amine CEST-EPI contrast using immunohistochemistry.

Materials and Methods

Patient Selection

This prospective study was approved by the Institutional Review Board at University of California Los Angeles under Institutional Review Board #10-000655 and #14-001261. All patients provided written informed consent for all clinical information, imaging exams, treatments, and prospective biopsy acquisition. A total of 30 patients were included in this study: Fifteen pathologically confirmed newly diagnosed IDH wild-type glioblastoma and 15 first recurrence IDH wild-type glioblastoma. The newly diagnosed IDH wild-type glioblastoma had no previous therapy, had radiologically confirmed gross total resection of the CE portion of tumor, and were treated with standard-of-care adjuvant temozolomide and radiation therapy. The recurrent IDH wild-type glioblastoma only had a single previous surgery and adjuvant standard of care temozolomide and radiation therapy without additional medical therapy, had radiologically confirmed gross total resection of the CE portion of tumor, and were treated with adjuvant CCNU. Recurrence was based on radiology reports of progressive enhancement on post-contrast T1-weighted images consistent with the modified RANO criteria. Additionally, all cases of potential progression were discussed in a multidisciplinary tumor board that included review of anatomic and physiologic imaging (eg, diffusion MRI, perfusion MRI, T1 subtraction maps, etc.) as well as clinical characteristics and previous treatment to verify the date of tumor progression. Cases noted to have recurrence and shown to have significant treatment effects after surgery (i.e. radiation necrosis,

pseudoprogression, etc.) were excluded from the current study.

Amine Chemical Exchange Saturation Transfer Echo Planar Imaging

Each patient was referred for amine chemical exchange saturation transfer echo planar imaging (CEST-EPI) imaging along with preoperative MRI within 1 week of planned surgery for tumor on a 3T Siemens Prisma or Skyra scanner (Siemens Healthcare, Erlangen, Germany). Standard of care brain tumor imaging preoperative sequences adhered to the standard brain tumor imaging protocol[33] and included at least a 1 mm 3D inversion-recovery gradient recalled echo images prior to and after injection of gadolinium contrast (Gd-DTPA, 0.1 mmol/kg) as well as dual-echo proton density/T2-weighted turbo spin echo images and T2-weighted FLAIR images with 3mm slice thickness and no interslice gap, as well as 2mm isotropic resolution 64 direction diffusion tensor images and dynamic susceptibility contrast perfusion MRI acquired according to current recommendations.[34] Amine CEST-EPI was acquired and post-processed according to previously published protocols.[16,25–27,35] Briefly, amine CEST-EPI was composed of a nonselective saturation pulse train of three 100 milliseconds Gaussian pulses, with a peak amplitude of 6 μT and an inter-pulse delay of 5 milliseconds, followed by spoiling gradients before each EPI readout. Images had a field of view of 256 × 256 mm^2, matrix size of 128 × 128, slice thickness of 4mm. A total of 29 *z*-spectral points were acquired, densely sampled around the amine proton resonance frequency (+3.0 ppm), the reference frequency (–3.0 ppm), and the water resonance frequency (0 ppm). We additionally performed a reference (S_0) scan with 4 averages using identical sequence parameters and no saturation pulse. Total scan time was approximately 5–7 minutes. CEST-EPI were then post-processed by (1) motion correction using affine transformation (*mcflirt*; Functional MRI of the Brain Software Library, Oxford, United Kingdom), (2) B_0 inhomogeneity correction using a *z*-spectra-based *k*-means clustering and Lorentzian fitting algorithm; X, and (3) calculation of MTR_{asym} at amine proton resonance frequency as a measure related to tissue acidity. MTR_{asym} at 3.0 ppm was defined using the equation: $MTR_{asym}(3.0\ ppm) = S(-3.0\ ppm)/S_0 - S(+3.0\ ppm)/S_0$, where $S(\omega)$ is the water MR signal available following the saturation pulses with offset frequency ω and S_0 is the reference signal acquired without RF saturation. An integral of width of 0.4 ppm was quantified around both –3.0 and + 3.0 ppm (–3.2 to –2.8 ppm and + 2.8 to + 3.2 ppm, respectively) spectral points, in order to improve signal-to-noise. All images were registered to post-contrast T1-weighted and T2-weighted FLAIR images for subsequent analyses.

Construction of CEST Positive NE Regions of Interest

CEST-positive NE regions of interest (CEST + NE ROI) were created using the Analysis of Functional NeuroImages (AFNI) software package.[36] First, CE tumor (CE) was segmented using contrast-enhanced T1-weighted digital subtraction as previously described,[37–39] where contrast enhancement was quantified by a positive signal intensity after voxel-wise subtraction pre-contrast T1-weighted images from post-contrast images. Following CE tumor segmentation, central necrotic and/or cystic regions were filled within the CE ROI (*AFNI; 3dmask_tool, dilate*). NE ROIs were then identified by dilating the CE ROI (*AFNI, 3dmask_tool, dilate*) in areas that overlap with T2 hyperintensity on FLAIR images. The purpose of this ROI was to capture the T2 hyperintensity that may include both vasogenic edema and NE infiltrating tumor cells. NE ROIs were filtered by MTR_{asym} values from CEST-EPI. Using previously described MTR_{asym} values of normal-appearing white matter, T2 hyperintense regions, CE regions, and necrotic regions of glioma,[26] we quantified acidic tissue (CEST positive, or "CEST+") as having an MTR_{asym} threshold of between 1.50% and 4.00%. These bounds were determined by median MTR_{asym} of normal-appearing white matter (0.7%), T2 hyperintensity (1.7%), and CE regions (2.9%) from our prior work,[26,35,40] as well as noise from non-tumor structures (lateral ventricle). Similar to previous work quantitatively studying T2 regions,[41] median MTR_{asym} in CEST + NE ROIs and volume of CEST + NE ROIs normalized by volume of CE tumor (*CEST + NE ROI volume/ CE ROI volume*) were quantified and used for further analyses. This normalization was done to control for bias contributed to the association between CE volume and survival, and achieve a comparison similar to that of Figure 2A-B, where radiographic differences are primarily attributed to differences in CEST + NE regions.[39,42,43]

Acquisition of Prospective Biopsy Targets in CEST + NE ROI

In patients undergoing surgery for glioma in whom preoperative CEST-EPI imaging was obtained, prospective biopsy targets were planned in the CEST + NE ROI. A 5 mm diameter spherical biopsy target was placed in the CEST + NE ROI and median MTR_{asym} within this region was quantified. This 3D object was transferred to intraoperative neuronavigation software (*BrainLab Elements, BrainLab Surgical Navigation System, Munich, Germany*) and uploaded to the intraoperative neuronavigation system (*BrainLab Curve, BrainLab Surgical Navigation System, Munich, Germany*). During resection of the tumor, biopsy specimens were identified and removed, and screenshots were acquired to confirm proper localization within the operating room. These specimens were immediately sent to pathology for storage and processing.

Immunohistochemical Staining and Evaluation

Biopsy specimens were paraffin-embedded and prepared for immunohistochemical (IHC) staining. Each specimen was stained for: (1) hematoxylin and eosin only, (2) Ki-67, (3) CD8, (4) CD31. These blocks were reviewed for quality control and whole slide images were captured and sent for analysis on QuPath (*Aperio Technologies, Vista, CA*).[44]

H and E slides were evaluated for whole cell density, Ki-67 slides were evaluated for percentage of positive nuclei, and CD8/CD31 were evaluated for percentage of positive cells.

Statistical Methods

All statistical tests were performed on GraphPad Prism (version 9.0.0 for Mac, GraphPad Software, San Diego, California, USA, www.graphpad.com). Sample size calculation for biopsy targets showed a sample size of 20 with expected change in cell density of 50% would provide approximate power of 80% at the 0.05 significance level. Survival analyses were carried out using Cox proportional hazard modeling and Kaplan–Meier analysis with reporting of median survival and Log-Rank *P*-value. Comparisons between CEST + NE ROI and patterns of recurrence were evaluated with chi-square analysis. Immunohistochemical staining and MTR_{asym} were compared using unpaired *t*-tests as well as linear regression analysis with reporting of Pearson *r* value. A linear regression model was generated using the equation below:

$$Cellularity\left[\text{cells}/\text{mm}^2\right] = A * (MTR_{asym} at\ 3ppm[\%]) + B$$

Using neuropathological diagnosis as the gold standard, a MTR_{asym} value of ≥ 1.5% was evaluated as a diagnostic test for presence of tumor cells. True positives, true negatives, false positives, and false negatives were calculated. Sensitivity, specificity, positive predictive value, and negative predictive value were calculated from these data. *P*-values ≤.05 were considered statistically significant.

Results

Amine CEST-EPI in CE Regions of Glioblastoma

In 30 patients (*patient demographics in* Table 1) with IDH-wild-type glioblastoma, the median MTR_{asym} *at 3 ppm* was calculated for CE tumor (Figure 1A-B). No differences in MTR_{asym} *at 3 ppm* were observed between newly diagnosed (*n = 15*) and recurrent (*n = 15*) IDH wild-type glioblastoma (*mean 2.88 vs. 2.27, unpaired t-test P = .193;* Figure 1C).

In newly diagnosed glioblastoma patients, there was no difference in progression-free survival (PFS) by median *MTRasym at 3 ppm* using a Cox proportional hazard model (*HR = 1.07; P = .717*) or when stratified by the median value of the cohort (*median PFS 0.80 vs. 0.70 years, log-rank P = .773,* Figure 1D*).* There was no difference in overall survival (OS) by median *MTRasym at 3 ppm* using a Cox proportional hazard model (*HR = 0.78; P = .258*) or when stratified by the median value of the cohort (*median OS 1.70 vs. 1.60 years, log-rank P = .474,* Figure 1E*).*

In recurrent glioblastoma patients, there was no difference in PFS by median *MTRasym at 3 ppm* using a Cox proportional hazard model (*HR = 1.41; P = .321*) or when stratified by the median value of the cohort (*median PFS 0.20 vs. 0.90 years, log-rank P = .148,* Figure 1F*).* There was no difference in OS by median *MTRasym at 3 ppm* using a Cox proportional hazard model (*HR = 1.17; P = .713*) or when stratified by the median value of the cohort (*median OS 1.60 vs. 1.70 years, log-rank P = .732,* Figure 1G*).*

Amine CEST-EPI in NE Regions of Glioblastoma

CEST + NE ROIs were created for all gliomas to identify potential areas of NE tumor as indicated by elevated tumor acidity. Interestingly, CEST + NE ROIs did not have complete overlap with the T2/FLAIR hyperintensity, and there was heterogeneity in the median MTR_{asym} and volume (Figure 2A-B). Median MTR_{asym} *at 3 ppm* of CEST + NE of grade IV IDH wild-type glioblastoma was lower than of the CE region (*2.09 vs. 2.63, paired t-test P = .0176,* Figure 2C). There were no differences in median MTR_{asym} *at 3 ppm* or volume ratio of CEST + NE ROIs between new and recurrent wild-type glioblastoma (*median MTR_{asym} 2.13 vs. 2.05 unpaired t-test P = .387,* Figure 2E*; volume ratio 1.05 vs. 0.70 unpaired t-test P = .366,* Figure 2F).

CEST + NE ROI Characteristics are Associated With Spatial Areas of Tumor Recurrence and PFS

In 15 newly diagnosed IDH wild-type glioblastoma patients and 15 recurrent IDH wild-type glioblastoma patients, Cox Proportional Hazard Regression was used to evaluate PFS and OS by median MTR_{asym} *at 3 ppm* of CEST + NE ROI (*newly diagnosed PFS HR = 2.31, P = .021; OS HR = 0.73, P = .737; recurrent PFS HR = 3.61, P = .297; OS HR = 0.33, P = .487*). Kaplan–Meier survival analysis of PFS and OS stratified by median MTR_{asym} *at 3 ppm* CEST + NE ROI showed significantly lower PFS with higher MTR_{asym} *at 3 ppm* in both groups of patients, but no difference in OS (*newly diagnosed median PFS 0.2 vs. 1.4 years, log-rank P = .0007,* Figure 3A*; OS 1.6 vs. 1.7 years log-rank P = .230,* Figure 3B*; recurrent median PFS 0.3 vs. 1.5 years, log-rank P = .020,* Figure 3C*; OS 1.6 vs.1.7 years, log-rank P = .456,* Figure 3D). Cox Proportional Hazard Regression of PFS and OS by CEST + NE ROI/ CE ROI volume ratio showed association of poor PFS with higher ratio (*newly diagnosed PFS HR = 1.56, P = .046; OS HR = 1.75, P = .061; recurrent PFS HR = 1.55, P = .128; OS HR = 1.77, P = .079).* Kaplan–Meier survival analysis by CEST + NE ROI/ CE ROI volume ratio showed significantly lower PFS with higher ratio (*newly diagnosed median PFS 0.2 vs. 0.9 years log-rank P = .033,* Figure 3E*; OS 1.3 vs. 1.7 years log-rank P = .388,* Figure 3F*; recurrent PFS 0.2 vs 1.7 years log-rank P < .0001,* Figure 3G*; OS 0.9 vs. 4.0 years log-rank P = .0003,* Figure 3H). In 22 IDH wild-type glioblastoma patients with GTR and follow-up imaging showing CE progression, 21/22 (95.4%) had recurrence in an area of CEST + NE ROI (*chi-square P < .001*). Illustrative examples include those with CEST + NE ROI well beyond the CE region of tumor with conversion to CE tumor on 1 year follow-up (Figure 3I), patients with very small areas of CEST + NE ROI without CE recurrence on 1 year follow-up (Figure 3J), and patients with CEST + NE ROI distant to the CE region with localized recurrence on 1 year follow up (Figure 3K).

Tumor and Non-tumor Cell Burden Correlates With MTR_{asym} at 3 ppm in CEST + NE ROI

A total of 14 patients with IDH-wild-type glioblastoma received successful MR-guided biopsies within CEST + NE ROIs to yield 20 individual samples (Figure 4A, *patient demographics* Table 2). A blinded, board-certified

Table 1. Patient Characteristics for Survival Analysis

Pt	Age	Gender	New vs. Recurrent	Diagnosis	IDH1/2 Mutation	1p/19q Loss	EGFR Amp	PTEN Loss	MGMT Methyl
1	49	M	New	GBM WHO 4	–	–	+	+	–
2	75	M	New	GBM WHO 4	–	–	-	+	+
3	65	M	New	GBM WHO 4	–	–	+	+	–
4	68	F	New	GBM WHO 4	–	–	+	+	+
5	56	M	New	GBM WHO 4	–	–	–	+	–
6	36	M	New	GBM WHO 4	–	–	+	+	–
7	67	M	New	GBM WHO 4	–	–	+	+	–
8	61	F	New	GBM WHO 4	–	–	–	+	+
9	60	M	New	GBM WHO 4	–	–	–	+	+
10	86	F	New	GBM WHO 4	–	–	–	+	+
11	66	F	New	GBM WHO 4	–	–	–	+	–
12	70	M	New	GBM WHO 4	–	–	+	+	+
13	70	F	New	GBM WHO 4	–	–	–	+	–
14	75	M	New	GBM WHO 4	–	–	+	+	+
15	51	M	New	GBM WHO 4	–	–	–	+	–
16	44	M	Recurrent	GBM WHO 4	–	–	–	+	–
17	61	F	Recurrent	GBM WHO 4	–	–	–	+	–
18	52	F	Recurrent	GBM WHO 4	–	–	–	+	+
19	56	M	Recurrent	GBM WHO 4	–	–	+	+	+
20	54	M	Recurrent	GBM WHO 4	–	–	+	–	+
21	46	M	Recurrent	GBM WHO 4	–	–	–	+	+
22	60	M	Recurrent	GBM WHO 4	–	–	+	+	–
23	60	F	Recurrent	GBM WHO 4	–	–	+	+	–
24	62	F	Recurrent	GBM WHO 4	–	–	+	+	+
25	51	F	Recurrent	GBM WHO 4	–	–	+	+	–
26	55	M	Recurrent	GBM WHO 4	–	–	+	+	+
27	41	F	Recurrent	GBM WHO 4	–	–	–	+	–
28	67	F	Recurrent	GBM WHO 4	–	–	–	+	+
29	78	M	Recurrent	GBM WHO 4	–	–	+	+	–
30	53	M	Recurrent	GBM WHO 4	–	–	–	–	–

neuropathologist reviewed randomized H&E stained slides of each of these 20 samples and provided a diagnosis of either (1) solid tumor, (2) infiltrating tumor, or (3) no tumor. The MTR_{asym} *at 3 ppm* of these samples correlated with the pathological diagnosis (*solid tumor mean* MTR_{asym} *= 2.36%; infiltrating tumor mean* MTR_{asym} *= 1.88%; no tumor mean* MTR_{asym} *at 3 ppm = 1.41%; ANOVA P = .0028,* Figure 4B). Cell density using a quantitative image analysis tool (*QuPath, Aperio Technologies*) showed a positive linear correlation between MTR_{asym} *at 3 ppm* and cell density (*pearson r = 0.801; P < .001,* Figure 4C) and a significant difference with a median stratification between high and low MTR_{asym} *at 3 ppm* (*4951 vs. 1082 cells/ mm^2; unpaired t-test P < .001,* Figure 4D). The mean cell density of slides deemed to be non-pathological brains was 811 cells/mm^2. A linear regression equation from this data were generated:

$$\text{Cellularity}\ \left[\text{cells/mm}^2\right] = 3793 * (MTR_{asym} at\ 3ppm[\%]) - 4453$$

Having a cellularity matching that of non-pathological brain is estimated to have a baseline MTR_{asym} *at 3 ppm* of 1.38%. Given these data, we used a cut-off of a MTR_{asym} of ≥ 1.50%. Using pathological diagnosis as the gold standard, we see a threshold of 1.50% as able to identify tumor cells with a sensitivity of 100%, specificity of 71.4%, positive predictive value of 86.7%, and negative predictive value of 100%.

There was positive linear correlation between MTR_{asym} *at 3 ppm* and the proportion of nuclei with positive Ki-67 staining (*pearson r = 0.834; P < .0001,* Figure 4E) and a significant difference with a median stratification between high and low MTR_{asym} (*26.7% vs. 2.7%; unpaired t-test P = .004,* Figure 4F). Staining against CD8 was used to quantitate levels of CD8$^+$ T-cells. There was no significant correlation between proportion of cells positive for CD8 and MTR_{asym} (*pearson P = .594; median stratified t-test P = .614,* Figure 4G-H). There was a significant correlation between proportion of cells positive for CD31, used to

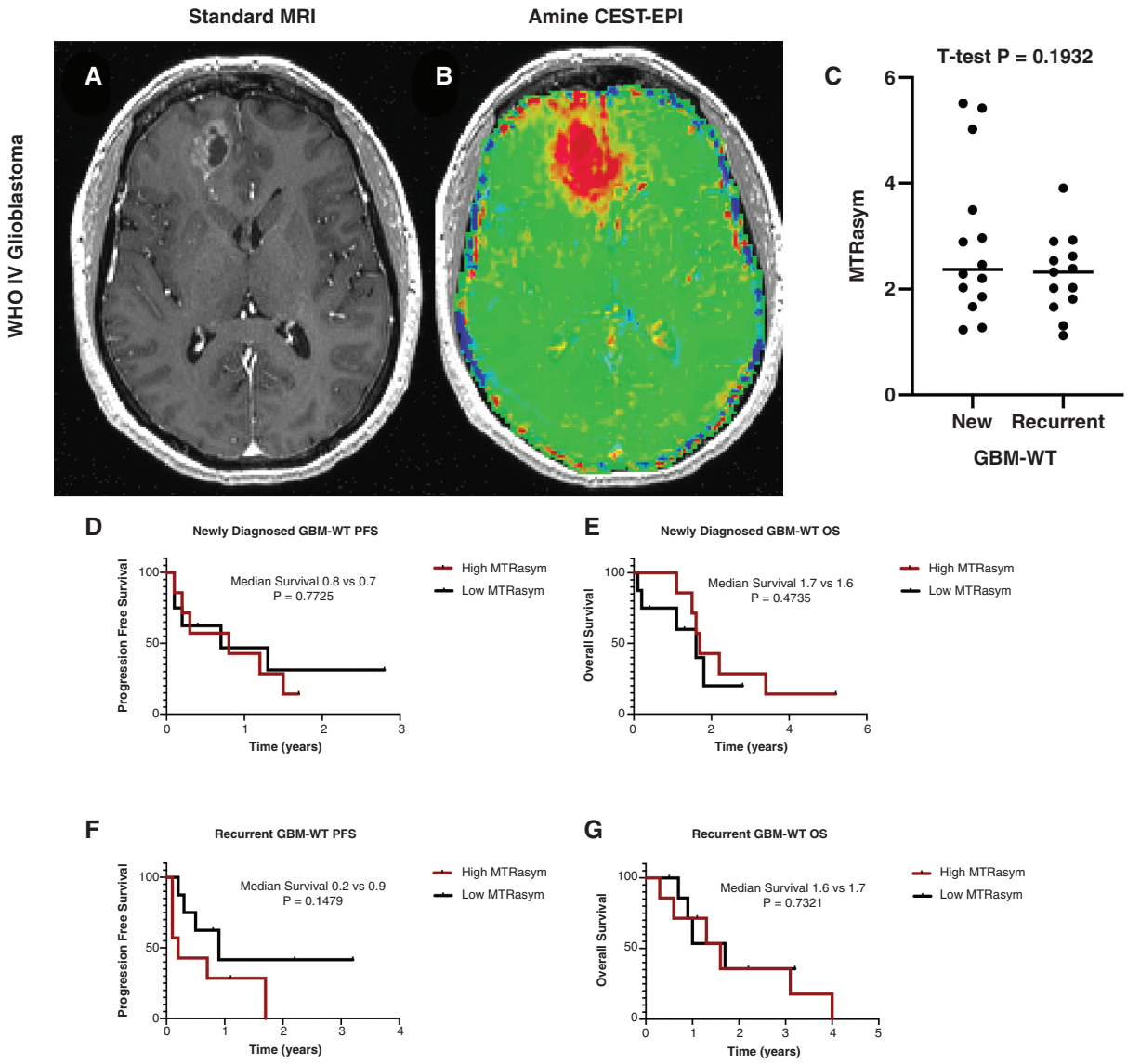

Figure 1. T1-weighted with contrast (A) and amine chemical exchange saturation transfer echo planar imaging (CEST-EPI) (B) sequences of WHO IV glioblastoma. Median MTR_{asym} of contrast-enhancing region in new and recurrent glioblastoma (C). Kaplan–Meier curves evaluating MTR_{asym} of the contrast-enhancing region in newly diagnosed glioblastoma progression-free survival (D), overall survival (E), recurrent glioblastoma progression-free survival (F), and overall survival (G).

quantitate levels of endothelial cells and *MTR_{asym} at 3 ppm* (*pearson r = 0.708; P = .001,* Figure 4I*);* and when stratified by median *MTR_{asym} at 3 ppm*, (*9.0% vs. 1.8%; t-test P = .006,* Figure 4J).

Discussion

In this study, we show the feasibility of amine CEST-EPI in identifying differences in *MTR_{asym} at 3 ppm* within the CE region as well as in areas beyond the CE region. We build upon previous work studying amine CEST-EPI in the CE regions of gliomas,[16,25–27,35] by constructing an automated pathway for identifying abnormality in the NE region, allowing for more information than previously studied CE regions of glioma. There is a clinical need for visualization of NE tumors. Standard T1 in contrast fails to visualize tumors in areas of intact blood-brain barrier.[45] T2 or FLAIR hyperintensity often extends much farther past the tumor and is thought to be cerebral edema. Identifying areas of this region that harbor infiltrating tumor cells has been studied with radiomic evaluation.[46,47] Scola et al. review standard and advanced techniques for evaluating this region including[19] While standard MRI studies can quantify NE low-grade gliomas,[48] and prognosticate high-grade gliomas,[49] confirmation with biopsies is lacking. In regards to alternative imaging techniques, FDG PET,

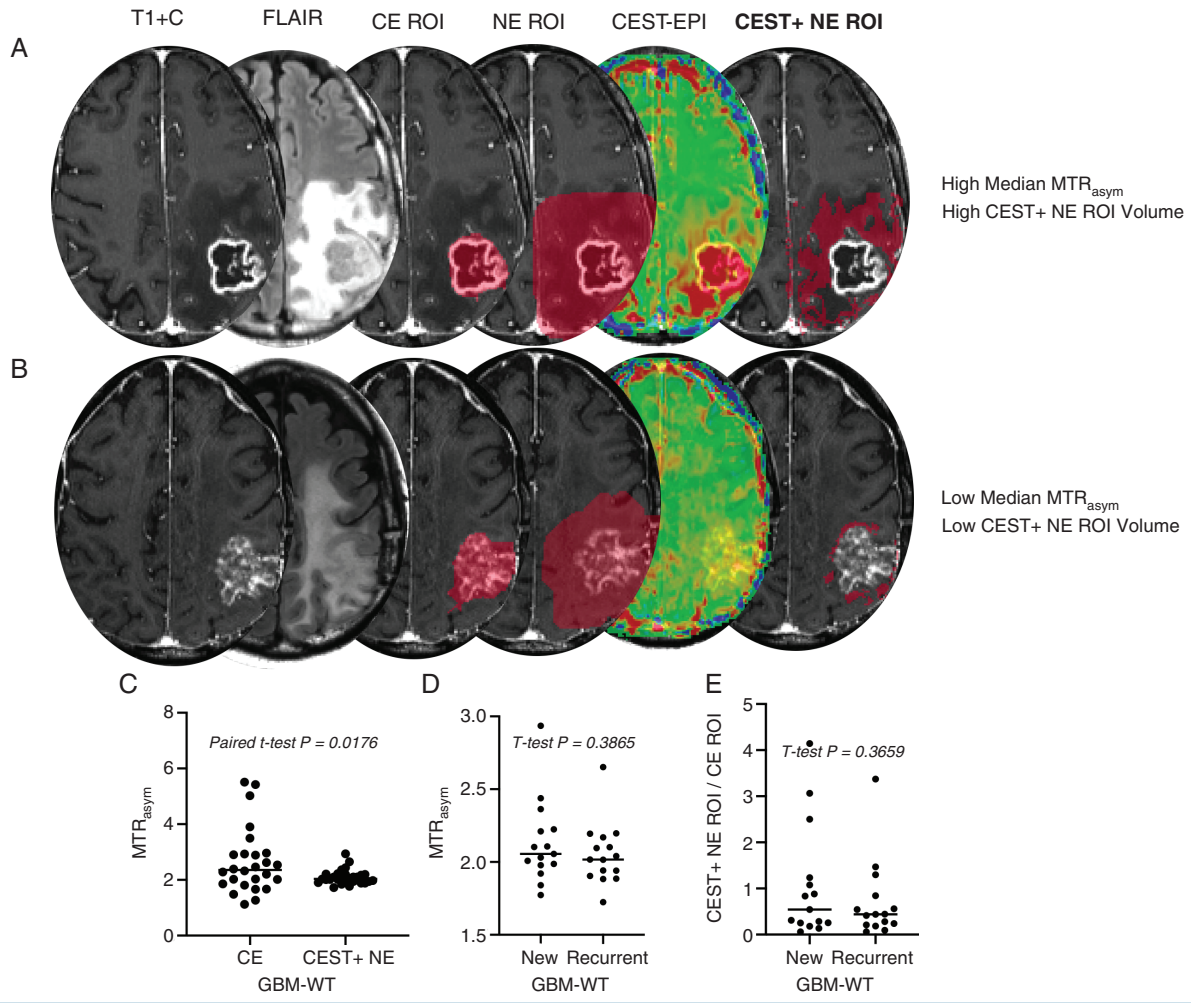

Figure 2. Quantitative segmentation pipeline for generation of CEST + non-enhancing (NE) regions of interest (ROI) with examples of high (A) and low (B) CEST + NE ROI. Median MTR$_{asym}$ of contrast-enhancing (CE) and NE areas of tumor (C). Median MTR$_{asym}$ of CEST + NE ROI in new and recurrent glioblastoma (D). Raio of CEST + NE ROI to CE ROI in new and recurrent glioblastoma.

perfusion-weighted imaging, diffusion-weighted imaging, diffusion tensor imaging, and MR spectroscopy have been studied to differentiate glioma from alternative diagnoses[18–20] and prognosticate outcome,[22,39] but resolution is extremely low and therefore cannot be leveraged by intraoperative neuronavigation.[15] Amine CEST-EPI identifies abnormality beyond the CE but not the entire extent of the FLAIR or T2. Although heterogeneous between patients, amine CEST-EPI abnormality follows white matter tracts. We show in this study a streamlined post-processing technique for amine CEST-EPI to identify areas beyond the CE region with abnormal *MTR$_{asym}$ at 3 ppm*, "CEST+ NE ROI," and introduce to quantitative measures for these ROIs: median *MTR$_{asym}$ at 3 ppm* and volume normalized by CE volume. Furthermore, amine CEST-EPI has near whole-brain coverage with 4mm slices, and *MTR$_{asym}$ at 3 ppm* color maps can be registered to the MP-RAGE images used in the intraoperative neuronavigation software.

CEST + NE ROI metrics were strongly associated with decreased progression-free survival (PFS) in IDH wild-type glioblastoma. We hypothesize that if infiltrating glioblastoma cells exist in this area, the larger this area (as denoted by volume of ROI), the more residual tumor, as standard of care surgery is resection of CE tumor only.[2–5,10] Similarly, the higher the median MTR$_{asym}$, the more metabolically active this residual tumor. This suggests that the term "recurrent glioblastoma" is actually capturing *progression* of NE infiltrating glioblastoma into higher density CE glioblastoma. In our newly diagnosed cohort, there was no difference in OS based on CEST + NE ROI volume. In our academic brain tumor center, these patients often receive multiple surgeries and trials and therefore depending on the arm of a trial and whether the family decided to pursue surgery is a large confounding factor for OS. In our recurrent cohort, we did see a significant association of CEST + NE ROI volume with PFS and OS, as these patients were much less likely to receive additional treatment upon progression other than palliative bevacizumab.

We sought to confirm the presence of tumor cells in CEST + NE ROIs by using prospective image-guided

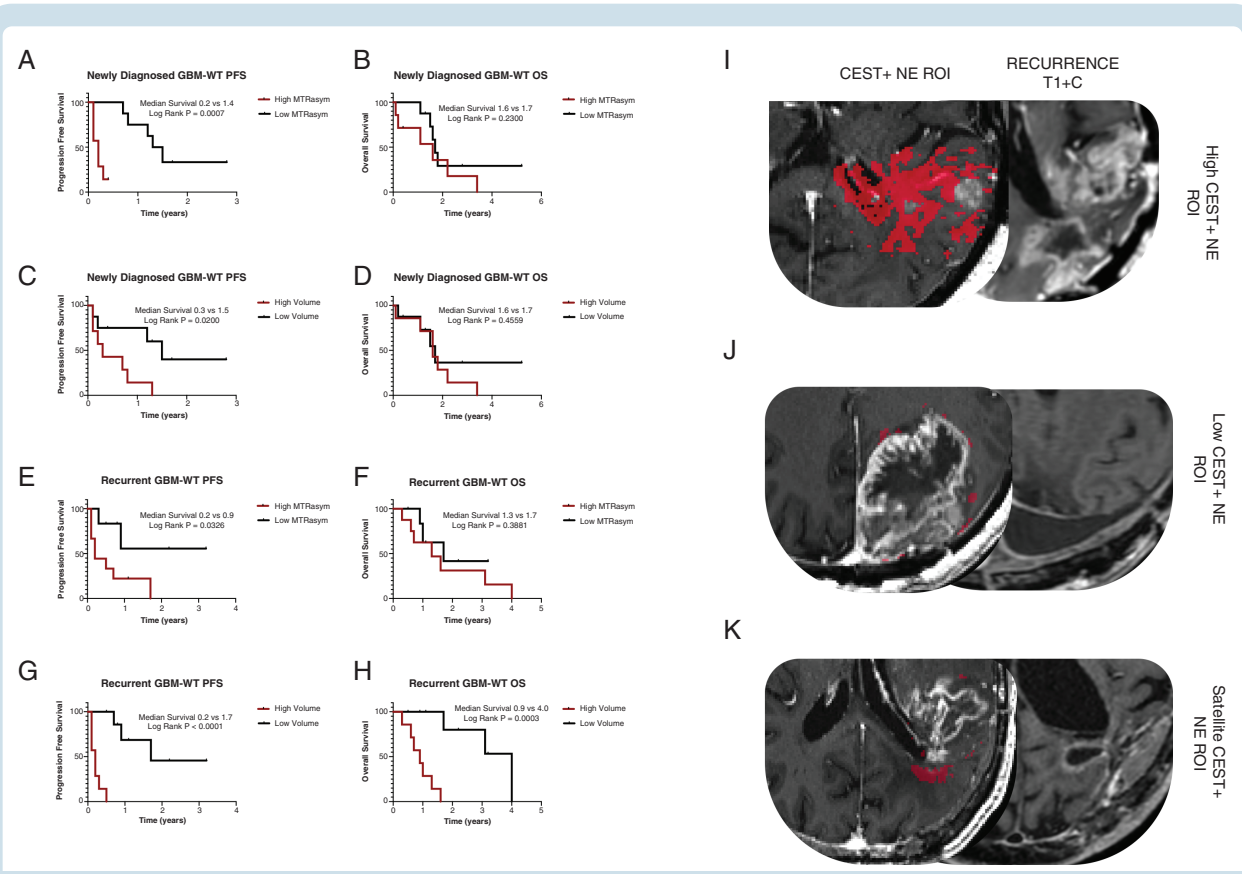

Figure 3. Kaplan–Meier survival curves in newly diagnosed (A–D) and recurrent (E–H) glioblastoma evaluating median MTR_{asym} of CEST + non-enhancing (NE) ROI (A–B, E–F) or volume ratio of CEST + NE ROI: CE ROI (C–D, G–H) on progression-free survival (PFS) (A, C, E, G) or overall survival (OS) (B, D, F, H). CEST + NE ROI on initial presentation and contrast-enhancing recurrence on follow-up showing high (I), low (J), or satellite (K) CEST + NE ROI.

Table 2. Patient Characteristics for IHC Analysis

Pt	Age	Gender	New vs. Recurrent	Diagnosis	IDH1/2 Mutation	1p/19q Loss	EGFR Amp	PTEN Loss	MGMT Methyl
1	75	M	New	GBM WHO 4	–	–	–	+	+
2	45	M	New	GBM WHO 4	–	–	–	+	–
3	68	F	New	GBM WHO 4	–	–	+	+	+
4	65	M	New	GBM WHO 4	–	–	+	+	–
5	36	M	New	GBM WHO 4	–	–	+	+	–
6	62	M	New	GBM WHO 4	–	–	–	+	+
7	62	M	New	GBM WHO 4	–	–	–	+	–
8	82	M	New	GBM WHO 4	–	–	+	–	+
9	44	M	Recurrent	GBM WHO 4	–	–	–	+	+
10	65	M	Recurrent	GBM WHO 4	–	–	–	+	+
11	69	M	Recurrent	GBM WHO 4	–	–	–	–	–
12	78	M	Recurrent	GBM WHO 4	–	–	+	+	+
13	67	F	Recurrent	GBM WHO 4	–	–	+	+	+
14	58	M	Recurrent	GBM WHO 4	–	–	+	+	–

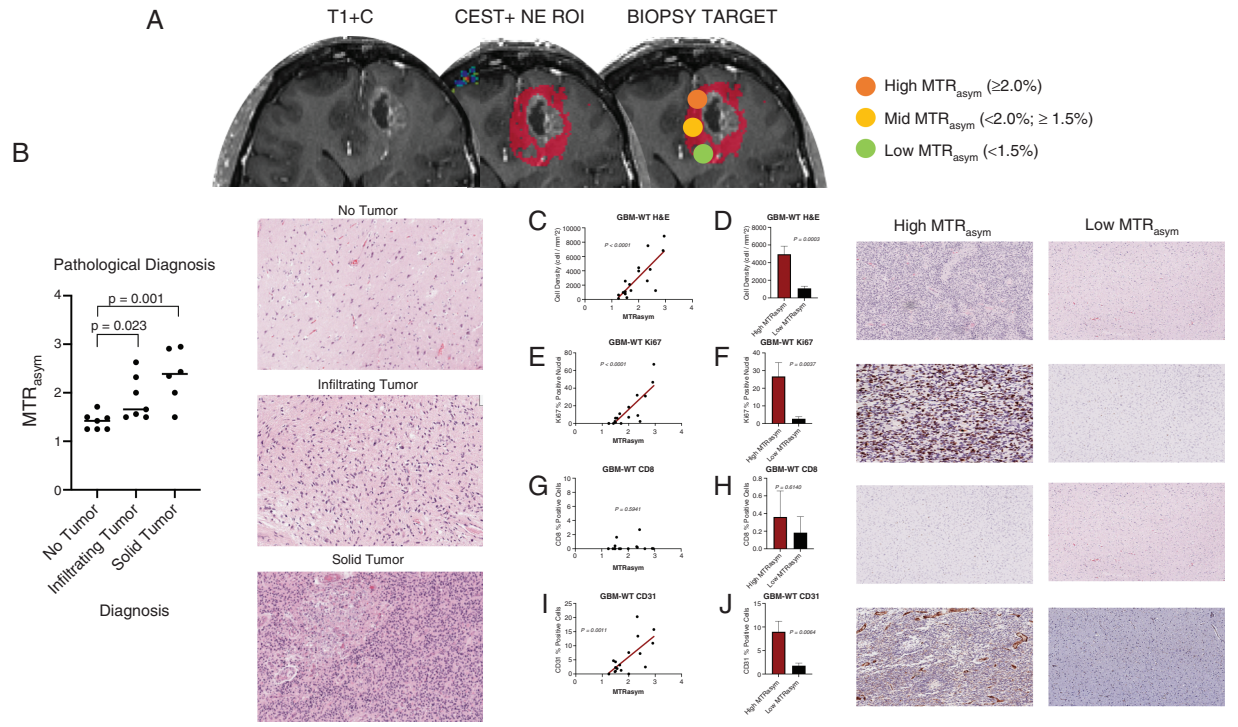

Figure 4. Prospective guided biopsies pipeline showing selection of areas of high/mid/low MTR$_{asym}$ in CEST + non-enhancing ROIs (A). Correlation of pathological diagnosis with MTR$_{asym}$ of biopsy target (B). Linear correlation (C, E, G, I) and median stratified comparison (D, F, H, J) of positive cell count in high or low MTR$_{asym}$ for cellular density on H&E (C–D), Ki-67 (E–F), CD8 (G–H), and CD31 (I–J).

biopsies of these regions and quantitating tumor cell burden via IHC. Using pathological diagnosis as the gold standard, we see a threshold of 1.50% as able to identify tumor cells with sensitivity. Furthermore, tumor cell density correlated with *MTR$_{asym}$ at 3 ppm*, where an estimated *MTR$_{asym}$ at 3 ppm* ≥ 1.41% was predictive of tumor cells. With these data, we hypothesize using a threshold of 1.50% can better visualize NE tumors, and guide surgeons to establishing an improved minimal residual disease baseline.

We began to address the question as to what is contributing to abnormal *MTR$_{asym}$ at 3ppm* in NE regions. We show in this study differences in tumor cell burden, and have previously shown differences in metabolism.[28] We hypothesize that *MTR$_{asym}$ at 3 ppm* abnormalities are due to (1) neoplastic cell burden and turnover, (2) intratumoral differences in metabolism (ie, aerobic glycolysis or the Warburg Effect[30,31,50]), or (3) immune response. Using IHC, we identify *MTR$_{asym}$ at 3 ppm* in CEST + NE ROI is associated with % Ki-67 and CD31^{+} positivity but not % CD8^{+} positivity. In fact, there are low CD8^{+} cells (<1%) identified throughout CEST + NE ROIs. This suggests that CEST + NE regions of tumors have active replication and vascular proliferation without evidence of a cell-mediated immune response. This makes this population of cells, likely those that remain after surgery, potential originators of recurrence and true target of adjuvant therapy.

This study has several limitations. The first is that there are multiple sources of bias that may lead to false positives/false negatives. CEST voxel size still limits resolution as compared to high-resolution MRI. Second, translation of prospective biopsy targets to real brain space in the operating room is difficult given shifts in cerebrospinal fluid and brain during exposure of the tumor. While we use neuro-pathologic review as the gold standard for defining negative tissue, individual infiltrating tumor cells may be present, a known limitation of defining margins in glioma. The second limitation extends to the applicability of this method. CEST sequences require significant post-processing, and interpretation in the operating room requires a surgeon with significant experience with this imaging modality. Differences in MRI scanners, contrast administration, and processing in different centers may lead to heterogeneity in application. In addition, with limited sample size, specifically for areas of low MTR$_{asym}$, true sensitivity, and specificity may benefit from further external validation. Lastly, our prognostic evaluation would be improved by measurement of actual post-operative NE tumors. This is an area of active further study. Additional future directions include correlating with additional MRI sequences, studying cell burden, RNA expression patterns, and microenvironment in these regions with single-cell sequencing and consideration of surgical trials to resect CEST + NE regions of glioblastoma to achieve a minimal disease post-operative state.

Conclusions

We introduce a novel method to visualize NE tumor cells using amine CEST-EPI. We investigate the relationship of our metrics to tumor characteristics and find these metrics as strongly associated with PFS. We confirm that CEST + NE ROIs do contain tumor cells and this is correlated with MTR_{asym} *at 3ppm*. Lastly, we show that MTR_{asym} *at 3 ppm* correlates with markers of cell turnover and differences in metabolism rather than presence of an immune response. We suggest that amine CEST-EPI can help visualize infiltrating tumor cells for further study of residual tumors after surgery.

Keywords

CEST-EPI | glioblastoma | non-enhancing | pH MRI

Funding

DoD CA20029 (Ellingson); R01CA270027 (Ellingson); NIH/NINDS R01NS078494 (Ellingson); P50CA211015 (Liau); NIGMS T32 GM008042 (Cho; Tessema); Neurosurgical Research Education Fund YCI KL2TR001882 (Patel).

Conflict of interest statement

BME is on the advisory board and is a paid consultant for Medicenna, MedQIA, Servier Pharmaceuticals, Siemens, Janssen Pharmaceuticals, Imaging Endpoints, Kazia, Oncoceutics/Chimerix, Sumitomo Dainippon Pharma Oncology, ImmunoGenesis, Ellipses Pharma, Monteris, Neosoma, Alpheus Medical, Sagimet Biosciences, Sapience Therapeutics, and the Global Coalition for Adaptive Research (GCAR).

Authorship statement

Study Conception: K.P., B.E. Data Acquisition: K.P., J.Y., F.R., R.E., L.L., B.E. Data Analysis/Interpretation: K.P., J.Y., N.C., F.S., K.T., A.A., L.D., F.R., H.K., B.E. Manuscript Generation: K.P., H.K., B.E. Figure Generation: K.P., J.Y., N.C. Critical Revision: K.P., J.Y., N.C., F.S., K.T., A.A., L.D., F.R., R.E., L.L., H.K., B.E. Study Supervision: F.R., R.E., L.L., H.K., B.E.

Data availability

Data will be made available upon reasonable request.

Affiliations

Department of Neurosurgery, David Geffen School of Medicine, University of California Los Angeles, Los Angeles, California, USA (K.S.P., R.E., L.L., B.M.E.); UCLA Brain Tumor Imaging Laboratory, Center for Computer Vision and Imaging Biomarkers, University of California Los Angeles, Los Angeles, California, USA (K.S.P., J.Y., N.S.C., F.S., B.M.E.); The Intellectual and Developmental Disabilities Research Center and Department of Psychiatry and Biobehavioral Sciences, David Geffen School of Medicine, University of California Los Angeles, Los Angeles, California, USA (K.S.P., K.T., A.A., L.D., H.K.); Department of Radiological Sciences, David Geffen School of Medicine, University of California Los Angeles, California, USA (J.Y., N.S.C., F.S., N.S., B.M.E.); Medical Scientist Training Program, David Geffen School of Medicine, University of California, Los Angeles, Los Angeles, California, USA (N.S.C., K.T.); Department of Bioengineering, Henry Samueli School of Engineering and Applied Science, University of California Los Angeles, Los Angeles, California, USA (N.S.C., B.M.E.); Department of Pathology, David Geffen School of Medicine, University of California Los Angeles, Los Angeles, California, USA (F.R.); Department of Neurology, David Geffen School of Medicine, University of California Los Angeles, Los Angeles, California, USA (T.F.C.)

References

1. Louis DN, Perry A, Wesseling P, et al. The 2021 WHO Classification of Tumors of the Central Nervous System: A summary. *Neuro Oncol*. 2021;23(8):1231–1251.
2. Stupp R, Mason WP, van den Bent MJ, et al; European Organisation for Research and Treatment of Cancer Brain Tumor and Radiotherapy Groups. Radiotherapy plus concomitant and adjuvant temozolomide for glioblastoma. *N Engl J Med*. 2005;352(10):987–996.
3. Sanai N, Polley MY, McDermott MW, Parsa AT, Berger MS. An extent of resection threshold for newly diagnosed glioblastomas. *J Neurosurg*. 2011;115(1):3–8.
4. Awad AW, Karsy M, Sanai N, et al. Impact of removed tumor volume and location on patient outcome in glioblastoma. *J Neurooncol*. 2017;135(1):161–171.
5. Brown TJ, Brennan MC, Li M, et al. Association of the extent of resection with survival in glioblastoma: A systematic review and meta-analysis. *JAMA Oncol*. 2016;2(11):1460–1469.
6. Gzell C, Back M, Wheeler H, Bailey D, Foote M. Radiotherapy in Glioblastoma: The Past, the Present and the Future. *Clin Oncol (R Coll Radiol)*. 2017;29(1):15–25.
7. Ellingson BM, Wen PY, Cloughesy TF. Evidence and context of use for contrast enhancement as a surrogate of disease burden and treatment response in malignant glioma. *Neuro Oncol*. 2018;20(4):457–471.
8. Shidoh S, Savjani RR, Cho NS, et al. Relapse patterns and radiation dose exposure in IDH wild-type glioblastoma at first radiographic recurrence following chemoradiation. *J Neurooncol*. 2022;160(1):115–125.
9. Vollmann-Zwerenz A, Leidgens V, Feliciello G, Klein CA, Hau P. Tumor cell invasion in glioblastoma. *Int J Mol Sci* . 2020;21(6):1932.

10. Molinaro AM, Hervey-Jumper S, Morshed RA, et al. Association of maximal extent of resection of contrast-enhanced and non-contrast-enhanced tumor with survival within molecular subgroups of patients with newly diagnosed glioblastoma. *JAMA Oncol.* 2020;6(4):495–503.
11. Paw I, Carpenter RC, Watabe K, Debinski W, Lo HW. Mechanisms regulating glioma invasion. *Cancer Lett.* 2015;362(1):1–7.
12. Bette S, Barz M, Huber T, et al. Retrospective analysis of radiological recurrence patterns in glioblastoma, their prognostic value and association to postoperative infarct volume. *Sci Rep.* 2018;8(1):4561.
13. Rakovec M, Khalafallah AM, Wei O, et al. A consensus definition of supratotal resection for anatomically distinct primary glioblastoma: An AANS/CNS Section on Tumors survey of neurosurgical oncologists. *J Neurooncol.* 2022;159(2):233–242.
14. Tripathi S, Vivas-Buitrago T, Domingo RA, et al. IDH-wild-type glioblastoma cell density and infiltration distribution influence on supramarginal resection and its impact on overall survival: A mathematical model. *J Neurosurg.* 2021;136(6):1–9.
15. Drake LR, Hillmer AT, Cai Z. Approaches to PET imaging of glioblastoma. *Molecules.* 2020;25(3):568.
16. Yao J, Hagiwara A, Raymond C, et al. Human IDH mutant 1p/19q co-deleted gliomas have low tumor acidity as evidenced by molecular MRI and PET: A retrospective study. *Sci Rep.* 2020;10(1):11922.
17. Altieri R, Certo F, Pacella D, et al. Metabolic delineation of IDH1 wild-type glioblastoma surgical anatomy: How to plan the tumor extent of resection. *J Neurooncol.* 2023;162(2):417–423.
18. Caravan I, Ciortea CA, Contis A, Lebovici A. Diagnostic value of apparent diffusion coefficient in differentiating between high-grade gliomas and brain metastases. *Acta Radiol.* 2018;59(5):599–605.
19. Scola E, Del Vecchio G, Busto G, et al. Conventional and advanced magnetic resonance imaging assessment of non-enhancing peritumoral area in brain tumor. *Cancers (Basel).* 2023;15(11):2992.
20. Sternberg EJ, Lipton ML, Burns J. Utility of diffusion tensor imaging in evaluation of the peritumoral region in patients with primary and metastatic brain tumors. *AJNR Am J Neuroradiol.* 2014;35(3):439–444.
21. Vallatos A, Al-Mubarak HFI, Birch JL, et al. Quantitative histopathologic assessment of perfusion MRI as a marker of glioblastoma cell infiltration in and beyond the peritumoral edema region. *J Magn Reson Imaging.* 2019;50(2):529–540.
22. Ricci R, Bacci A, Tugnoli V, et al. Metabolic findings on 3T 1H-MR spectroscopy in peritumoral brain edema. *AJNR Am J Neuroradiol.* 2007;28(7):1287–1291.
23. Di Costanzo A, Trojsi F, Tosetti M, et al. High-field proton MRS of human brain. *Eur J Radiol.* 2003;48(2):146–153.
24. Harris RJ, Cloughesy TF, Liau LM, et al. pH-weighted molecular imaging of gliomas using amine chemical exchange saturation transfer MRI. *Neuro Oncol.* 2015;17(11):1514–1524.
25. Harris RJ, Cloughesy TF, Liau LM, et al. Simulation, phantom validation, and clinical evaluation of fast pH-weighted molecular imaging using amine chemical exchange saturation transfer echo planar imaging (CEST-EPI) in glioma at 3 T. *NMR Biomed.* 2016;29(11):1563–1576.
26. Harris RJ, Yao J, Chakhoyan A, et al. Simultaneous pH-sensitive and oxygen-sensitive MRI of human gliomas at 3 T using multi-echo amine proton chemical exchange saturation transfer spin-and-gradient echo echo-planar imaging (CEST-SAGE-EPI). *Magn Reson Med.* 2018;80(5):1962–1978.
27. Cho NS, Hagiwara A, Yao J, et al. Amine-weighted chemical exchange saturation transfer magnetic resonance imaging in brain tumors. *NMR Biomed.* 2022;36(6):e4785.
28. Hagiwara A, Yao J, Raymond C, et al. "Aerobic glycolytic imaging" of human gliomas using combined pH-, oxygen-, and perfusion-weighted magnetic resonance imaging. *NeuroImage Clin.* 2021;32:102882.
29. Yao J, Wang C, Ellingson BM. Influence of phosphate concentration on amine, amide, and hydroxyl CEST contrast. *Magn Reson Med.* 2021;85(2):1062–1078.
30. Nguyen TTT, Shang E, Shu C, et al. Aurora kinase A inhibition reverses the Warburg effect and elicits unique metabolic vulnerabilities in glioblastoma. *Nat Commun.* 2021;12(1):5203.
31. Poteet E, Choudhury GR, Winters A, et al. Reversing the Warburg effect as a treatment for glioblastoma. *J Biol Chem.* 2013;288(13):9153–9164.
32. Garcia JH, Jain S, Aghi MK. Metabolic drivers of invasion in glioblastoma. *Front Cell Dev Biol.* 2021;9:683276.
33. Ellingson BM, Bendszus M, Boxerman J, et al; Jumpstarting Brain Tumor Drug Development Coalition Imaging Standardization Steering Committee. Consensus recommendations for a standardized Brain Tumor Imaging Protocol in clinical trials. *Neuro Oncol.* 2015;17(9):1188–1198.
34. Boxerman JL, Quarles CC, Hu LS, et al; Jumpstarting Brain Tumor Drug Development Coalition Imaging Standardization Steering Committee. Consensus recommendations for a dynamic susceptibility contrast MRI protocol for use in high-grade gliomas. *Neuro Oncol.* 2020;22(9):1262–1275.
35. Yao J, Tan CHP, Schlossman J, et al. pH-weighted amine chemical exchange saturation transfer echoplanar imaging (CEST-EPI) as a potential early biomarker for bevacizumab failure in recurrent glioblastoma. *J Neurooncol.* 2019;142(3):587–595.
36. Cox RW. AFNI: Software for analysis and visualization of functional magnetic resonance neuroimages. *Comput Biomed Res.* 1996;29(3):162–173.
37. Ellingson BM, Kim HJ, Woodworth DC, et al. Recurrent glioblastoma treated with bevacizumab: Contrast-enhanced T1-weighted subtraction maps improve tumor delineation and aid prediction of survival in a multicenter clinical trial. *Radiology.* 2014;271(1):200–210.
38. Patel KS, Yao J, Raymond C, et al. Decorin expression is associated with predictive diffusion MR phenotypes of anti-VEGF efficacy in glioblastoma. *Sci Rep.* 2020;10(1):14819.
39. Patel KS, Everson RG, Yao J, et al. Diffusion magnetic resonance imaging phenotypes predict overall survival benefit from bevacizumab or surgery in recurrent glioblastoma with large tumor burden. *Neurosurgery.* 2020;87(5):931–938.
40. Cho NS, Hagiwara A, Yao J, et al. Amine-weighted chemical exchange saturation transfer magnetic resonance imaging in brain tumors. *NMR Biomed.* 2023;36(6):e4785.
41. Naeini KM, Pope WB, Cloughesy TF, et al. Identifying the mesenchymal molecular subtype of glioblastoma using quantitative volumetric analysis of anatomic magnetic resonance images. *Neuro Oncol.* 2013;15(5):626–634.
42. Ellingson BM, Harris RJ, Woodworth DC, et al. Baseline pretreatment contrast enhancing tumor volume including central necrosis is a prognostic factor in recurrent glioblastoma: Evidence from single and multicenter trials. *Neuro Oncol.* 2017;19(1):89–98.
43. Ellingson BM, Abrey LE, Nelson SJ, et al. Validation of postoperative residual contrast-enhancing tumor volume as an independent prognostic factor for overall survival in newly diagnosed glioblastoma. *Neuro Oncol.* 2018;20(9):1240–1250.
44. Bankhead P, Loughrey MB, Fernández JA, et al. QuPath: Open source software for digital pathology image analysis. *Sci Rep.* 2017;7(1):16878.
45. Steeg PS. The blood-tumour barrier in cancer biology and therapy. *Nat Rev Clin Oncol.* 2021;18(11):696–714.
46. Parvaze S, Bhattacharjee R, Singh A, et al. Radiomics-based evaluation and possible characterization of dynamic contrast enhanced (DCE) perfusion derived different sub-regions of Glioblastoma. *Eur J Radiol.* 2023;159:110655.

47. Pati S, Verma R, Akbari H, et al. Reproducibility analysis of multi-institutional paired expert annotations and radiomic features of the Ivy Glioblastoma Atlas Project (Ivy GAP) dataset. *Med Phys.* 2020;47(12):6039–6052.
48. Zhu Z, Gong G, Wang L, et al. Three-dimensional arterial spin labeling-guided sub-volume segmentation of radiotherapy in adult non-enhancing low-grade gliomas. *Front Oncol.* 2022;12:914507.
49. Tippareddy C, Onyewadume L, Sloan AE, et al. Novel 3D magnetic resonance fingerprinting radiomics in adult brain tumors: A feasibility study. *Eur Radiol.* 2023;33(2):836–844.
50. Zhang Y, Nguyen TTT, Shang E, et al. MET inhibition elicits PGC1α-dependent metabolic reprogramming in glioblastoma. *Cancer Res.* 2020;80(1):30–43.